PCCP

PAPER

View Article Online
View Journal | View Issue

Cite this: *Phys. Chem. Chem. Phys.*, 2018, **20**, 20812

Strong light–matter interaction in tungsten disulfide nanotubes†

Lena Yadgarov,[ab] Bojana Višić,[ac] Tsafrir Abir,[bd] Ron Tenne,[e] Alexander Yu. Polyakov,[f] Roi Levi,[a] Tatyana V. Dolgova,[g] Varvara V. Zubyuk,[g] Andrey A. Fedyanin,[g] Eugene A. Goodilin,[f] Tal Ellenbogen,[d] Reshef Tenne[a] and Dan Oron*[e]

Received 9th April 2018,
Accepted 29th June 2018

DOI: 10.1039/c8cp02245c

rsc.li/pccp

Transition metal dichalcogenide materials have recently been shown to exhibit a variety of intriguing optical and electronic phenomena. Focusing on the optical properties of semiconducting WS_2 nanotubes, we show here that these nanostructures exhibit strong light–matter interaction and form exciton–polaritons. Namely, these nanotubes act as quasi 1-D polaritonic nano-systems and sustain both excitonic features and cavity modes in the visible-near infrared range. This ability to confine light to subwavelength dimensions under ambient conditions is induced by the high refractive index of tungsten disulfide. Using "finite-difference time-domain" (FDTD) simulations we investigate the interactions between the excitons and the cavity mode and their effect on the extinction spectrum of these nanostructures. The results of FDTD simulations agree well with the experimental findings as well as with a phenomenological coupled oscillator model which suggests a high Rabi splitting of ~280 meV. These findings open up possibilities for developing new concepts in nanotube-based photonic devices.

1 Introduction

Over the last decade, vast research efforts have been devoted to understanding and utilizing the unique optical properties of semiconductor nanostructures (SC NS). In this context, much attention was drawn to their ability to confine light at nanoscale dimensions.[1–3] This feature results in increased electric field strength and thus enhances light–matter interaction, *i.e.* leads to strong nonlinearities, large photonic forces and enhanced emission and absorption probabilities.[4] Generally, the SC NS support cavity modes only if their length scales are comparable to the wavelength of light in a vacuum. However, semiconductors with high refractive index (RI) can also efficiently confine light in subwavelength dimensions.[4,5] The resonance conditions in semiconductor nanocavities depend on the refractive indices of the medium and the SC, the nanostructure's dimensions and geometry, as well as the polarization of the optical field. In addition to their ability to sustain cavity mode resonances (CMRs), the ability to generate excitons in high RI semiconductor nanostructures can be used to create quasi-particles known as exciton polaritons (EPs). EPs form as a result of coupling between the excitons and the optical modes of the nanocavity. The hybrid nature of EPs opens possibilities for applications associated with energy and information transfer, photonic and quantum technologies.[6–8]

Typically, the interaction between excitons and CMR is studied in the regimes of weak and strong coupling. The energy spectrum of the system is modified in both cases, *i.e.*, the frequencies of the new modes are different from those of the original oscillator modes. However, the difference between the original and the new frequencies depends on the strength of the coupling.[9] Weak coupling manifests itself as a narrow (minor) asymmetric dip at the resonance frequency of the uncoupled oscillators. In this regime, the shift due to coupling is negligible compared to the resonance frequencies of the underlying modes[9] and the energy transfer rate between the two modes is assumed to be smaller than the relaxation rate of the system.[10,11] In the strong coupling regime, the interaction between the modes is strong enough to significantly modify the

[a] *Department of Materials and Interfaces, Faculty of Chemistry, Weizmann Institute of Science, Rehovot 76100, Israel*
[b] *Department of Condensed Matter Physics, School of Physics and Astronomy, Tel Aviv University, Tel Aviv 69978, Israel*
[c] *Condensed Matter Physics Department, Jozef Stefan Institute, Jamova 39, 1000 Ljubljana, Slovenia*
[d] *Department of Physical Electronics, School of Electrical Engineering, Tel-Aviv University, Tel Aviv 69978, Israel*
[e] *Department of Physics of Complex Systems, Faculty of Physics, Weizmann Institute of Science, Rehovot 76100, Israel. E-mail: dan.oron@weizmann.ac.il*
[f] *Faculty of Materials Science, Lomonosov Moscow State University, Leninskie Gory 1-73, 119991 Moscow, Russia*
[g] *Faculty of Physics, Lomonosov Moscow State University, Leninskie Gory 1 bldg 2, 119991 Moscow, Russia*

† Electronic supplementary information (ESI) available. See DOI: 10.1039/c8cp02245c

energy levels. Strong coupling manifests itself as well-separated peaks in the energy spectrum. Here, the new energies correspond to modes that are hybrids of the original modes of the interacting oscillators.[9,12] The strong interaction between the coupled modes leads to an oscillation between the two excited states.[11] The period of this oscillation is known as Rabi oscillation period and should be shorter than the decoherence time of the excitation.[13]

Transition metal dichalcogenides (TMDC) materials of the type MX_2 (M = Mo, W; X = S, Se) have been intensively studied for many years. These layered materials have A, B and C exciton transitions in the visible light range. The excitonic transitions arise from the interlayer interactions and spin–orbit splitting[14] and the magnitude of the A–B splitting is independent of the number of layers.[15] Due to their sizable bandgaps, strongly bound excitons and high oscillator strength, these materials are expected to sustain stable polaritons at ambient conditions and thus become suitable for technological applications.[16–18] Indeed, it was shown that MX_2 embedded in microcavities exhibited signatures of strong EP coupling.[19] More recently, MX_2 TMDCs have emerged as unique systems supporting several types of polaritons with no external cavity.[20–24] The fact that EP can exist in multilayered TMDC materials under ambient conditions inspired a renewed interest in the optical properties of MX_2 closed-cage layered nanostructures.

Closed-cage multi-wall MX_2 nanostructures, such as nanotubes[25] and fullerene-like nanoparticles[26,27] have been synthesized in substantial amounts and their properties were widely studied. These studies resulted in numerous applications, *e.g.* for superior solid-state lubrication,[28–33] and led to their rapid commercialization. The multi-wall closed-cage MX_2 nanostructures preserve the semiconductor nature of their bulk counterparts and are usually indirect band gap semiconductors.[34,35] The large scale and robust synthesis of WS_2 nanotubes (NT) allows conducting systematic studies of such systems including their mechanical, optical and electronic properties.[36–39] For instance, quasi-1D superconductivity was recently found in the WS_2 nanotubes.[40] For a recent review on advances in studying and utilizing their properties (see ref. 41).

Although light–matter interaction of bulk and single layers of MX_2 materials is studied intensively, their closed caged counterparts have not been thoroughly explored yet. Notwithstanding, the study of excitons coupled with light in multilayered quasi 1D materials could provide broader perspectives for the fundamental properties of EP in subwavelength dimensions. Their stability and the lack of the dangling bonds can suppress exciton capture at non-radiative recombination centers, such as surface states and impurities. Moreover, WS_2 NT can provide additional benefits for applications and fundamental research requiring high-aspect ratio nanoparticles.

Here we report that WS_2 nanotubes can sustain excitonic and cavity modes at room temperature. The overlap between these two modes can lead to strong coupling between the electronic transitions and the confined optical fields, resulting in the formation of exciton-polaritons. Using finite-difference time-domain (FDTD) simulations and a phenomenological coupled oscillator (PCO) model we confirm that their cavity resonance occurs in the visible-near-infrared spectral region, such that it can spectrally overlap with the A and B excitonic features of the semiconductor. Indeed, the extinction spectra of the dispersed nanotubes exhibit the "signature" of a strong coupling, *i.e.* the two excitonic transitions of WS_2[42] turn into three peaks and none of them are in their original frequency. Moreover, the extinction spectrum shows prominent transparency dips at the spectral positions associated with the A (630 nm) and B (520 nm) excitons and a broad extinction band above 650 nm which is attributed to scattering.

2 Results and discussion

2.1 Absorbance and extinction spectra

The studied WS_2 nanotubes[43] consist of 20–40 concentric shells, span diameters between 40 to 150 nm and are typically 1 to 10 μm long.[36] Fig. 1a and b present typical scanning and transmission electron microscopy images of such nanotubes. The high degree of crystalline order of the nanotubes can be appreciated from these figures. Additionally, images of WS_2 NT

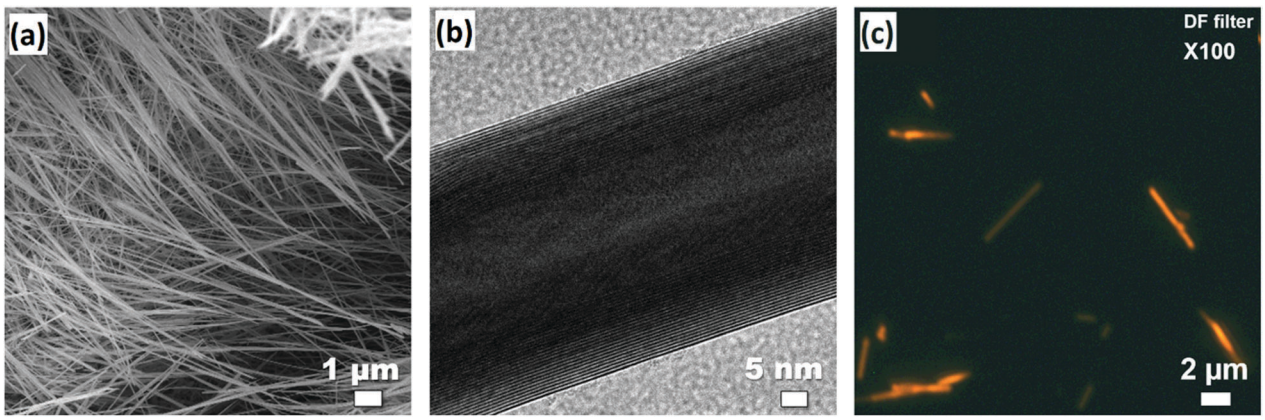

Fig. 1 Typical microscopy micrographs of WS_2 nanotubes. (a) Acquired using scanning electron microscope. (b) Acquired using transmission electron microscope. (c) Acquired using dark-field optical microscopy equipped with an optical filter that blocks the scattered light below 590 nm.

were acquired using dark-field optical microscopy equipped with an optical filter that blocks scattering below 590 nm (Fig. 1c). Despite the optical filter, and in the absence of photoluminescence, the nanotubes appearance is distinct and bright, indicating significant light scattering. Note that the experiments below rely only on extinction/reflection measurements since multilayered WS_2 is an indirect gap material[34,44,45] and as such does not exhibit any amount of measurable fluorescence.

Extinction and absorbance measurements were performed in an aqueous dispersion of the nanotubes using both a standard UV-vis spectrometer and an integrating sphere (Methods, Section II). The evolution from the absorption spectrum to the extinction spectrum was studied at intermediate configurations, where the sample is placed a short distance from the integrating sphere, as shown in the ESI,† Section S1 and Fig. S1.

Standard extinction measurements in a UV-vis spectrophotometer provide spectra which include contributions of both scattering and absorbance features. In contrast, the use of an integrating sphere allows measurement of the absolute absorption spectrum, excluding the scattering contribution. Hence, the resonances observed only in the absorption spectrum at 630 nm and 520 nm are assigned to the A and B excitonic transitions, respectively (Fig. 2a – black line).[45] Interestingly, although this spectrum is obtained without the scattering contribution, the excitonic peaks are very broad and somewhat quenched. These can be the result of broad span of NT sizes and some intrinsic defects in the NT (sulfur vacancies and dislocations), as well as due to a relatively high degree of defect-induced doping. In addition to excitons' spectral positions, the absorbance spectrum was used to derive the spin–orbit splitting and the direct and indirect-bandgaps of the WS_2 nanotubes. The derived values, presented in Table 1, are in good agreement with the literature.[14,34,42,46] The detailed description of the derivation of the bandgap and the spin–orbit splitting from the absorbance spectrum is shown in ESI,† Section S2.

The difference between the absorbance and the extinction spectra, *i.e.* the appearance of an extra peak and transparency dips in the extinction spectra (Fig. 2a), indicates that some interaction between an exciton and additional resonance occurs in this system (Fig. 2b). Moreover, it is clear from the measurements that these interactions originate from scattering rather than absorption of light.

2.2 Finite-difference time-domain extinction simulations

To elucidate the nature of this phenomenon, we studied the system numerically by performing FDTD simulations using a commercial solver (Lumerical FDTD solutions). Compared to the effective wavelengths of light within the NT (which has a refractive index of about 4), the length of the NT is long (>1 micron) and the diameter of the innermost tube is sufficiently small (<5–10 nm) to neglect the hollow tube at the center. This allows us to approximate the WS_2 NT as infinitely long cylindrical nanowire (NW).[47] For a qualitative representation of a "pure" cavity mode (without the contribution of the excitonic features), the simulation was performed using a constant refractive index (n = 4). To simulate the effect of the excitons, the dielectric function data of bulk WS_2 was used.[48] In both cases, the NW were irradiated separately by plane waves propagating in a direction perpendicular to the long

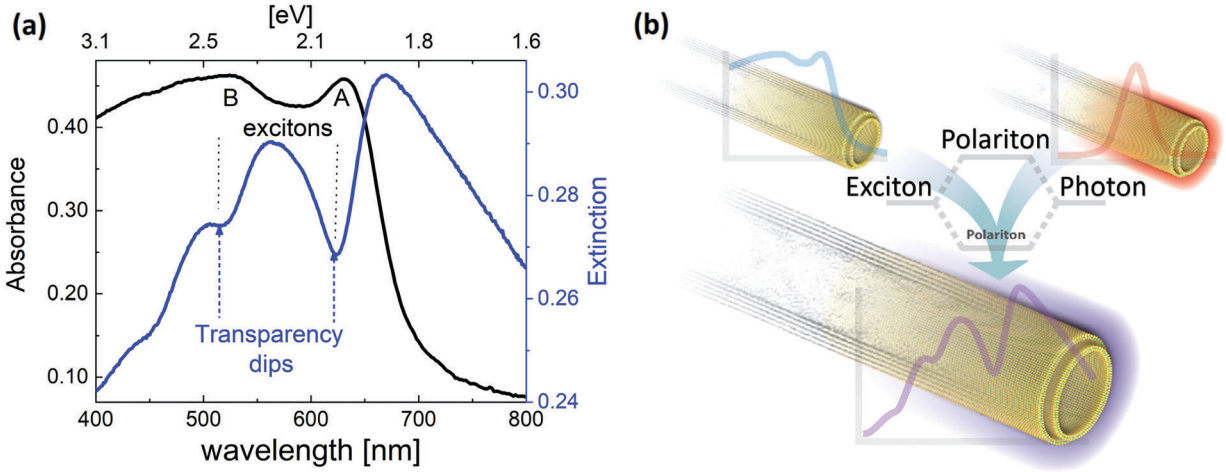

Fig. 2 Steady-state absorption and extinction spectra. (a) Comparison between the absolute absorbance (black) and extinction (blue) of WS_2 nanotubes dispersed in aqueous solution. (b) Schematic illustration of the strong coupling and hybridization of modes in the nanotubes.

Table 1 Summary of band gaps and exciton peak positions of WS_2 nanotubes dispersed in aqueous solution

	Excitons [eV]			Band gap [eV]	
	A	B	Spin orbit splitting [eV]	Direct	Indirect
Absolute absorbance	1.97 (629.4 nm)	2.39 (518.8 nm)	0.42	2.01	1.29
The literature values for bulk WS_2	1.95[46] (636.2 nm)	2.41[46] (514.5 nm)	0.43[46]	2.04[14,42]	1.30[34]

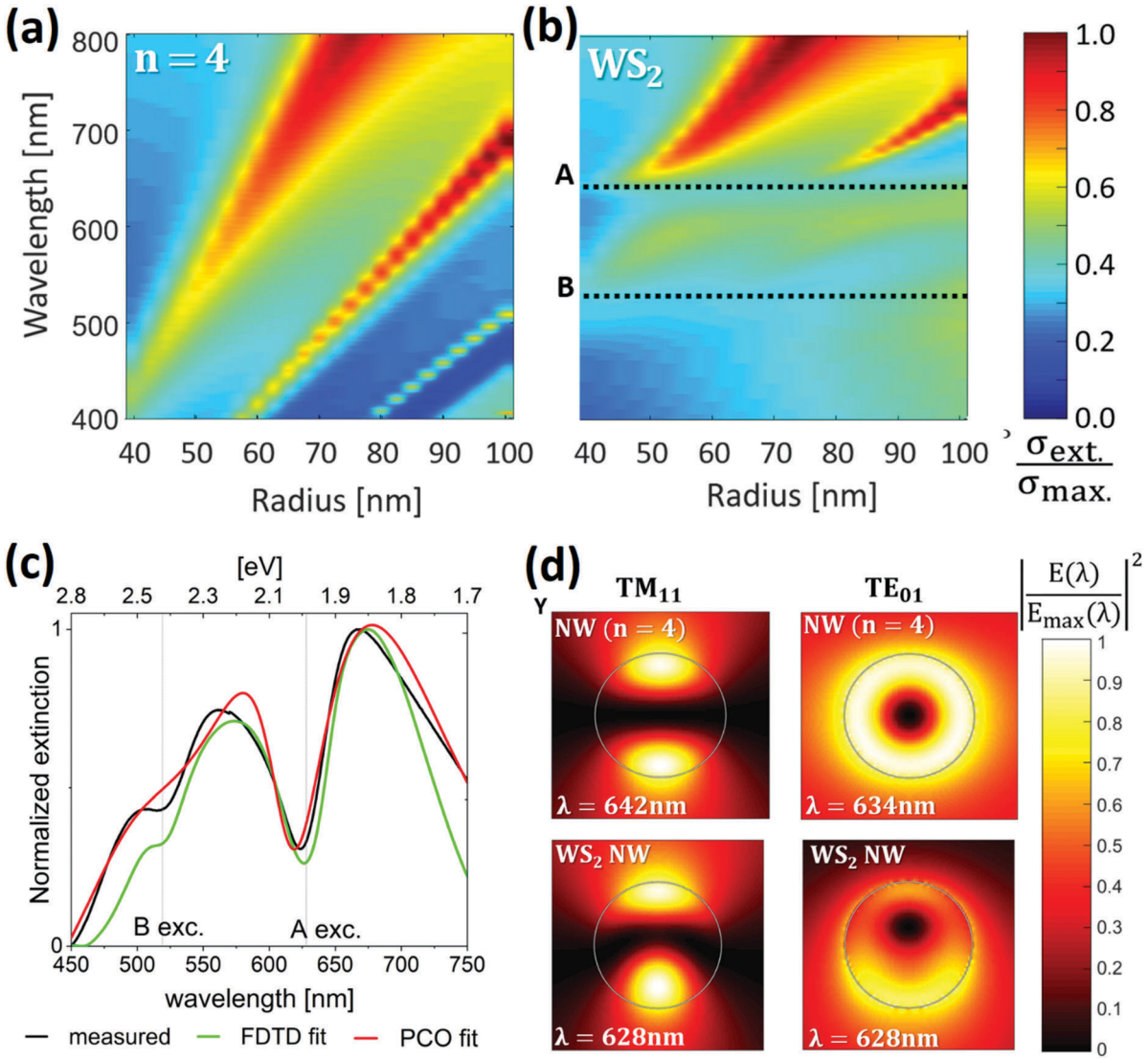

Fig. 3 Extinction spectra (wavelength *vs.* radii of the NW) simulated using FDTD (a) with constant refractive index (n_{NW} = 4) to qualitatively represent WS_2 NT without the effects of the excitons and (b) with the dielectric data of a bulk WS_2.[48] Splitting of the resonances can be recognized near the wavelength associated with A and B exciton resonances (horizontal black dotted line). The simulated irradiation is by plane waves polarized parallel to the nanotube long axis. (The extinction spectra perpendicular polarization is presented in ESI,† Section S4). (c) Comparison of fits obtained using PCO model (red) and FDTD (green) to the measured extinction spectra of the WS_2 NTs dispersed in aqueous solution (black). For the FDTD fit, average over the parallel and perpendicular polarizations and radii of the NW (40 to 65 nm) was performed to calculate the relevant extinction spectrum. (d) A map of the electric field's intensity for transverse magnetic/electric (TM/TE) modes of the NW (n = 4) and the WS_2 NW (r = 60 nm). The TM/TE modes corresponds to the parallel (TM) and perpendicular (TE) polarization to the wire's long axis (ESI,† Fig. S4). The values are normalized by the highest value recorded for both polarizations in each set separately. The sampled wavelengths are chosen to show the TM/TE modes around the A exciton transition.

axis of the cylinder and polarized parallel or perpendicular to it. The extinction cross-section calculated using the simulated electromagnetic field scattered and absorbed by the NW is shown in Fig. 3a and b and ESI,† Section S4.

The cavity mode resonances are clearly evident in the extinction spectra of NWs with different radii having all constant refractive index (n = 4) (Fig. 3a and ESI,† Section S4). Here, the high refractive index (compared to the surrounding) enables the NW to trap light by total internal reflection turning it into nano-cylindrical resonators which support cavity mode resonances.[4,5] As the radius increases the resonances are red-shifted and higher modes are supported. These findings are consistent with the previously observed CMRs in Ge NW, where modes were partially confined to the nanowire.[4] Interestingly, there is a high spectral overlap between the exciton modes of the NT and the simulated cavity modes of the $NW_{n=4}$ (r = 60 nm) (ESI,† Section S4 and Fig. S3d). The overlap between these modes is one of the main conditions for strong exciton–photon interaction and the formation of EP.

Once the WS_2's bulk dielectric function data is used for simulation, splitting of the cavity resonances can be recognized near the wavelength associated with the excitons (Fig. 3b and ESI,† Section S4). The features of the size-dispersive resonant modes are somewhat blurry for shorter wavelengths, due to

Table 2 The data derived from the PCO model fit to the measured extinction of the WS_2 nanotubes

λ [eV] (Wavelength)			γ [eV] (damping frequency, *i.e.* linewidth)			g [eV] (coupling strength)	
Scattering mode	Exciton A	Exciton B	Scattering mode	Exciton A	Exciton B	With exciton A	With exciton B
2.05 (604.5 nm)	1.99 (623 nm)	2.39 (518 nm)	0.80 (1.21×10^{15} Hz)	0.15 (2.26×10^{14} Hz)	0.52 (7.86×10^{14} Hz)	0.163 (2.46×10^{14} Hz)	0.175 (2.65×10^{14} Hz)

high absorption of the WS_2 NT in those wavelengths. The measured extinction spectrum was compared to the fitted one by averaging over the extinction for parallel and perpendicular polarizations and radii of the NT (40 to 65 nm). The results presented in Fig. 3c are in good agreement with the measured extinction and support the existence of strong light–mater interaction in the dispersed WS_2 NT. Interestingly, despite the fact that not all the orientations were taken into account, the good fit indicates that the main features of the extinction spectrum are captured by considering only the two extremal orientations. The splitting between the resonances in the fitted extinction spectra are 330 and 248 meV for cavity modes coupled to A and B excitons, respectively. These values are comparable to the Rabi splitting of EP in thin WS_2 flakes ($\sim$270 meV).[20] The map of the electric field's intensity at specific wavelengths was calculated for WS_2 nanowire with a radius of 60 nm (Fig. 3d and ESI,† Section S4). Note that the transverse magnetic/electric (TM/TE) modes are derived when the light polarizations are parallel/perpendicular to the NT's long axis. The calculated modes can be identified as the TM_{11} and TE_{01} modes.[4] Interestingly, although the TE modes are less intense than the TM modes, the overlap between the excitons and the TE cavity modes is higher (ESI,† Section S4 and Fig. S3c). Thus, it can be concluded that the TE and the TM modes both contribute to the observed extinction spectra.

2.3 Fitting with a coupled-oscillator model

The results of the FDTD simulation confirm the existence of cavity modes in the WS_2 NT. Moreover, the appearance of transparency dips[49] near the excitonic resonances implies that there is a strong interaction (coupling) between the CMR and the excitons. To obtain additional physical understanding of the apparent transparency dips, the extinction spectrum was fitted using a phenomenological coupled oscillator (PCO) model[50] (Fig. 3c, red line). Indeed, this fit supports the assumption that the extinction spectrum of WS_2 is dominated by strong coupling between the excitonic features and the cavity mode.

Generally, in the PCO model the ground state transitions are described as damped harmonic oscillators.[11] In the case of WS_2 nanotubes these oscillators represent the polarization of a cavity mode and the A and B excitonic transitions. The coupling between the cavity and excitonic oscillators is *via* a dipole–dipole energy term $E_{int} = 2g_i\omega_i x_i x_c$. Here x_i (i = A, B) is the exciton polarization, x_c is proportional to the cavity electrical field amplitude, ω_i is the exciton transition frequency and g_i is the exciton–cavity coupling strength. The coupling between the two (A and B) excitonic bands is assumed to be only mediated by the cavity mode.

Using such a modelling scheme, one can derive the expression for the extinction spectrum (see Methods, eqn (1) and ESI,† Section S3 for more details). The extinction spectrum of WS_2 NTs is fitted to the expression in eqn (1) and the results are presented in Fig. 3c and Table 2. The best fit is achieved when the energies of the two excitonic oscillators are in agreement with the A and B exciton energies, supporting the validity of the model. These results uphold the notion that the transparency dips observed in the WS_2 NT extinction spectrum are induced by hybridization of the excitons with the cavity mode. The coupling strengths, g_A and g_B, of the cavity mode with the A and B excitons respectively, are $\sim$163 meV and 175 meV (Table 2). These coupling strengths are comparable to those observed in WS_2 flakes (g_A = 135 meV and g_B = 390 meV).[20]

For a simple system consisting of two degenerate and undamped coupled oscillators, the extinction spectrum will consist of two sharp peaks. In this case, each of the peak energies corresponds to the hybrid mode energy. The splitting between the two energies is termed the Rabi energy splitting (Ω) and is related to the coupling constant by $\Omega_i = 2g_i$.[51] The NT system is more complicated as it includes three excited states (two excitonic states and a cavity state) which are non-degenerate and have non-negligible loss rates. Here, the values of the splitting are substantially different from $\Omega_i = 2g_i$ (which corresponds to $\sim$340 meV for both transitions). Consequently, for WS_2 NT the energy splitting (Ω) between the coupled modes was numerically derived using the resonant modes of the system and is Ω = 280 meV for the lowest energy states and Ω = 640 meV for the highest energy states (ESI,† Section S3.1).

2.4 Reflectivity of WS_2 nanotubes film

For further investigation of the excitons-CMR interactions, the reflectivity of a textured thin film consisting of WS_2 nanotubes deposited on a quartz substrate was measured. The micrographs of the film and the detailed scheme of the measurement setup are presented in ESI,† Section S7 and Fig. S6, S7. Schematic renderings of the two considered geometries for the reflection measurements are displayed in Fig. 4a. The electric field of the s-polarized (s-pol) incident light is perpendicular to the plane of incidence (parallel to the film plane independent of the angle). In contrast, the electric field of the p-polarized (p-pol) incident light is parallel to the plane of incidence, so that it is nearly parallel to the nanotube film at low (θ) angles, and nearly perpendicular to the film near grazing incidence. Thus, due to dielectric effects, at low (θ) angles both the p and the s polarized incident light the reflectivity spectrum will be dominated by the response to fields parallel to the nanotubes, and hence will be dominated by the excitonic response.[52,53]

The reflection spectra for the s- and p-polarizations at different irradiation angles[54] are presented in Fig. 4b. At low angles (5°) three maxima are observed at 640, 535, 475 nm for

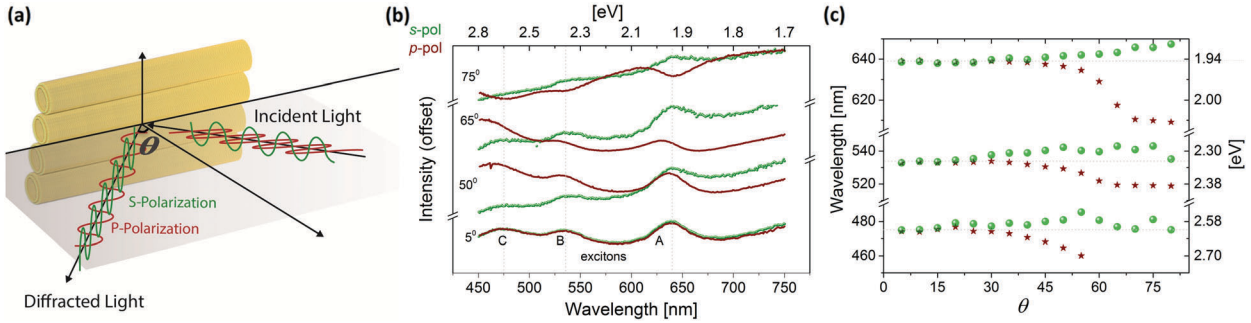

Fig. 4 Reflectivity of textured WS_2 nanotubes thin film. (a) Schematic representation of the two considered geometries. The electric field of the s-/p-polarized incident light is perpendicular/parallel (respectively) to the film plane and to the WS_2 nanotube *c*-axis. Note that the incident radiation is normal to the basal plane of the nanotube, *i.e.* the optic *E* vector is always perpendicular to the crystal *c*-axis ($E \perp c$ or $E \parallel a$).[59] (b) Comparison of the reflection spectra for the s- and p-polarizations at different angles (the given angles are between the incident beam propagation direction and the normal of the film). (c) The observed maxima positions of s- and p-polarized light as a function of angle. Note that when the incident light is p-polarized, the maxima are blue-shifted as the angle increases. Contrary, when the light is s-polarized, the maxima slightly red-shifts. This observation implies that CMR is excited only by the p-pol light.

both spectra, roughly matching the position of excitonic transitions in WS_2 NTs. For s-polarized light, these peaks are not expected to shift for higher angles since the electric field is always in the plane of the film. Indeed, the reflectivity spectrum of s-polarized light is nearly independent of angle. The maxima observed at 640, 535, 475 nm can be assigned to the A, B and C excitonic transitions (Fig. 4b).[45] The observed maxima are somewhat red-shifted compared to the ones obtained from the absorbance measurement (630, 520 and 450 nm). This shift may originate from multiple scattering within the nanotubes' film[55,56] or from a background that causes peak asymmetry.

In contrast, at high angle excitation with p-polarized light, the electric field is close to perpendicular to all the nanotubes in the film. Thus, the interaction of the p-polarized light at higher angles is dominated by coupling to the cavity mode. Indeed, the peaks are blue-shifted with increasing angle when the incident light is p-polarized. These blue-shifts become obvious above $\sim 60^\circ$, and when the incidence angle is 75° the maxima are at 610 and 524 nm (Fig. 4c). Moreover, the reflectance spectra for p-pol (80°) is comparable to the results of FDTD simulation for polarization perpendicular to the NT axis (ESI,† Section S6 and Fig. S6d). These results strengthen the conclusion that polaritonic effects are at work in these nanotubes.

3 Conclusions

We show that the WS_2 nanotubes emerge as a unique class of quasi 1D-material that is able to sustain both excitons and cavity modes in the visible and near IR spectral range. The diameter-dependent FDTD simulated extinction spectra exhibit a typical anti-crossing behavior and the formation of the exciton polaritons. These findings imply that the variation in the NTs' radius enables tunability of the coupling strength between the optical mode and the WS_2 excitons. By using the phenomenological coupled oscillator (PCO) model, the (Rabi) splitting between the coupled modes was evaluated to be as high as 280 meV.

The strong light–matter interaction in the WS_2 nanotubes suggests that they can be used for polaritonic devices at room temperature. Namely, the possibility of controlling the excitons resonances and hence that of the polaritons *via* gating, doping or variation of the NT radius opens possibilities for developing photonic devices with great potential for controllability. These findings hold a great promise for the studies of exciton-based light–matter interaction in TMDCs and their optical applications.

4 Experimental section

4.1 Materials

The multiwall WS_2 nanotubes used in the current work were purchased from "NanoMaterials Ltd" and were synthesized as pure phase according to the published procedures.[36] The synthesis was carried out at 800–950 °C using a mixture of different phases of WO_x ($2.83 \leq x \leq 3$) as precursors. These nanotubes have a typical average length of 1–10 μm and diameter of 50 to 100 nm (Fig. 1). The solutions for all the current measurements were prepared using purified (18 MOhm) water (Milli-Q RG, Millipore).

4.2 Steady-state absorption and extinction spectra

UV-vis extinction measurements were carried out using a Cary-5000 spectrometer (Varian). The samples were prepared by adding 0.6 mg of the WS_2 nanotubes into 9 ml of Milli-Q purified water. The mixture was hand-shaken and subsequently sonicated twice for 1–3 min using ultrasonic bath. All suspensions were measured using quartz cuvettes. Scanning electron microscopy (SEM) and transmission electron microscopy (TEM) analyses demonstrated that the nanotubes remain almost unaffected by this mild sonication procedure.

In order to separate the scattering and the absorption processes from the total extinction spectra we used an integrating sphere (Hamamatsu Quantaurus absolute QY measurement system).[57,58] This instrument directly measures the amount of absorbed light by placing the sample inside an integrating sphere. The system was calibrated using a sample with known absorbance to extract the optical absorbance. A calibration for counting the single-pass absorption photons was performed to avoid the full

extinction which also includes photons that are scattered a few times before being detected.

4.3 FDTD simulation

Finite-difference time-domain simulations were carried by a commercial solver of Maxwell's equations in time and space (Lumerical FDTD).

The nanowires' length is large compared to the relevant wavelengths and thus enable us to efficiently run two-dimensional simulation while still get meaningful results. The nanowires are simulated as infinitely long cylinders with different radii surrounded by an environment of constant refractive index similar to the solvent ($n_0 = 1.3$). Monitors were placed in the simulation to record the electromagnetic field scattered and absorbed by the nanowire. From these monitors the normalized extinction cross-sections were calculated. The normalization was with respect by the highest value recorded for both polarizations in each set, separately. Additional monitor was used in the simulation to measure the electric field in the region of the nanowire and identify the principal relevant CMRs. The simulations were performed for normal incidence, however the principal CMRs can be excited also at oblique incidence. Schematic description of 2D FDTD simulation setup can be found in ESI,† Section S4 and Fig. S4.

4.4 Fitting with a coupled-oscillator model

In the phenomenological coupled oscillator (PCO) model, used throughout this text, the ground state transitions described as damped harmonic oscillators coupled through an interaction term.[50] In the case of WS_2 nanotubes, the model was extended to include the two exciton bands (A and B) which couple to a cavity mode, ignoring the contribution of exciton *C*.

A simple derivation (ESI,† Section S3) yields an expression (eqn (1)) for the power loss by an incoming light beam impinging on a nanotubes solution (extinction) *versus* the beam's angular frequency (ω):

$$C_{\mathrm{ext}}(\omega) \propto \langle F_{\mathrm{CMR}}\dot{x}_{\mathrm{CMR}}\rangle \alpha \omega\ \mathrm{Im}\left\{\frac{D_{\mathrm{A}}(\omega)D_{\mathrm{B}}(\omega)}{D_{\mathrm{CMR}}(\omega)D_{\mathrm{A}}(\omega)D_{\mathrm{B}}(\omega) - 4\omega_{\mathrm{A}}{}^2\cdot g_{\mathrm{A}}{}^2 D_{\mathrm{B}}(\omega) - 4\omega_{\mathrm{B}}{}^2\cdot g_{\mathrm{B}}{}^2 D_{\mathrm{A}}(\omega)}\right\} \quad (1)$$

Here we define $D_{\mathrm{i}}(\omega) = \omega_{\mathrm{i}}{}^2 + \mathrm{i}\omega_{\mathrm{i}}\gamma_{\mathrm{i}} - \omega^2$, where the i subscript denotes parameters of either A, B or the SP which stand for the A exciton, B exciton and cavity mode respectively. ω_{i} and γ_{i} represent the resonance and damping frequency of the i oscillator respectively whereas the coupling strength between the i exciton band and the cavity mode is defined as g_{i}.

The expression presented in eqn (1) is used to fit the experimental extinction spectra in order to test the validity of the model in the case of WS_2 nanotubes and deduce the resonance frequencies.

4.5 Reflectivity measurements

For preparation of the WS_2 nanotubes film, the aqueous suspension of the nanotubes was mixed with 1/2 volume of heptane and sonicated in ultrasonic bath for 10 minutes. Within 30 min after sonication, the liquid phase segregates and nanotubes film forms on the liquid–liquid water–heptane interface. The high density of the nanotubes at the liquid–liquid interface; their high aspect ratio and low shear resistance allows the nanotubes to accommodate a somewhat parallel (textured) configuration. The nanotubes films could be easily transferred onto different substrates like quartz slides and silicon wafers, while maintaining their texture. The typical micrographs of WS_2 nanotubes film acquired using SEM and optical microscopy are presented in ESI,† Fig. S6 and Section S6.

The setup used for the angle/wavelength-dependent reflectivity measurements is shown in ESI,† Fig. S7 and Section S6. Halogen lamp was used as a light source. The initial light was collimated using the converging lenses and apertures were used to shape the beam into a parallel light source (2 mm in diameter). A Glan prism mounted on a precisely rotating support was used for controlling linear polarization of the incident light. The textured WS_2 nanotubes film deposited on a fused quartz slide was mounted on a motorized $\theta - 2\theta$ goniometer. The reflected beam was focused to an optical fiber mounted on a swivel mount of goniometer and connected to a Solar S100 spectrometer. The reflectivity spectra were collected using p-polarized and s-polarized incident light at 5–80° θ angles (5° step), 400–1050 nm wavelength range and 1 nm spectral resolution. In order to normalize the signal intensities in spectra obtained at different θ angles, the same measurements were carried out using 635 nm laser of fixed intensity. Afterwards, the spectra sets were normalized using the ratio of reflectivity intensities at given θ angle and 635 nm wavelength measured in laser and lamp experiments: $R_{\mathrm{laser}}(\theta;\ 635\ \mathrm{nm})/R_{\mathrm{lamp}}(\theta;\ 635\ \mathrm{nm})$.

Conflicts of interest

There are no conflicts of interest to declare.

Acknowledgements

This research was supported by the Israel Science Foundation Grants no. 265/12; the EU project ITN – "MoWSeS" (grant no. 317451); The Perlman Family Foundation; the Irving and Azelle Waltcher Foundation in honor of Prof. M. Levy (grant No. 720821). EAG and AYP acknowledge the support of the Russian Science Foundation (grant no. 14-13-00871); The Israel Science Foundation Israeli Center of Research Excellence "Circle of light" and the Crown Center for Photonics. AYP and EAG are grateful to Andrey A. Eliseev (Lomonosov MSU) for the help with the setup for integrating sphere measurements.

Notes and references

1 A. P. Alivisatos, *Science*, 1996, **271**, 933.
2 K. J. Vahala, *Nature*, 2003, **424**, 839.

3 R. K. Chang and A. J. Campillo, *Optical processes in microcavities*, World scientific, 1996.
4 L. Cao, J. S. White, J.-S. Park, J. A. Schuller, B. M. Clemens and M. L. Brongersma, *Nat. Mater.*, 2009, **8**, 643–647.
5 J. Hu and C. R. Menyuk, *Adv. Opt. Photonics*, 2009, **1**, 58–106.
6 C. Weisbuch, M. Nishioka, A. Ishikawa and Y. Arakawa, *Phys. Rev. Lett.*, 1992, **69**, 3314.
7 H. Gibbs, G. Khitrova and S. Koch, *Nat. Photonics*, 2011, **5**, 273.
8 F. Tassone, F. Bassani and L. Andreani, *Phys. Rev. B: Condens. Matter Mater. Phys.*, 1992, **45**, 6023.
9 P. Törmä and W. L. Barnes, *Rep. Prog. Phys.*, 2015, **78**, 013901.
10 R. Chance, A. Prock and R. Silbey, *Adv. Chem. Phys.*, 1978, **37**, 65.
11 L. Novotny, *Am. J. Phys.*, 2010, **78**, 1199–1202.
12 S. Haroche, in *Les Houches Summar School Session*, ed. J. D. e. Al, Amsterdam, North Holland, 1992, ch. 13, pp. 767–940.
13 J. Bellessa, C. Bonnand, J. C. Plenet and J. Mugnier, *Phys. Rev. Lett.*, 2004, **93**, 036404.
14 R. Coehoorn, C. Haas and R. De Groot, *Phys. Rev. B: Condens. Matter Mater. Phys.*, 1987, **35**, 6203–6206.
15 H. Zeng, G.-B. Liu, J. Dai, Y. Yan, B. Zhu, R. He, L. Xie, S. Xu, X. Chen and W. Yao, *Sci. Rep.*, 2013, 3.
16 A. Splendiani, L. Sun, Y. Zhang, T. Li, J. Kim, C.-Y. Chim, G. Galli and F. Wang, *Nano Lett.*, 2010, **10**, 1271–1275.
17 B. Radisavljevic, A. Radenovic, J. Brivio, V. Giacometti and A. Kis, *Nat. Nanotechnol.*, 2011, **6**, 147–150.
18 Q. H. Wang, K. Kalantar-Zadeh, A. Kis, J. N. Coleman and M. S. Strano, *Nat. Nanotechnol.*, 2012, **7**, 699–712.
19 S. Dufferwiel, S. Schwarz, F. Withers, A. Trichet, F. Li, M. Sich, O. Del Pozo-Zamudio, C. Clark, A. Nalitov and D. Solnyshkov, *Nat. Commun.*, 2015, 6.
20 Q. Wang, L. Sun, B. Zhang, C. Chen, X. Shen and W. Lu, *Opt. Express*, 2016, **24**, 7151–7157.
21 Z. Fei, M. Scott, D. Gosztola, J. Foley IV, J. Yan, D. Mandrus, H. Wen, P. Zhou, D. Zhang and Y. Sun, *Phys. Rev. B: Condens. Matter Mater. Phys.*, 2016, **94**, 081402.
22 F. Hu, Y. Luan, M. Scott, J. Yan, D. Mandrus, X. Xu and Z. Fei, *Nat. Photonics*, 2017, **11**, 356.
23 Y. Li, E. C. Moy, A. A. Murthy, S. Hao, J. D. Cain, E. D. Hanson, J. G. DiStefano, W. H. Chae, Q. Li and C. Wolverton, *Adv. Funct. Mater.*, 2018, **28**, 1704863.
24 A. A. Murthy, Y. Li, E. Palacios, Q. Li, S. Hao, J. G. DiStefano, C. Wolverton, K. Aydin, X. Chen and V. P. Dravid, *ACS Appl. Mater. Interfaces*, 2018, **10**, 6799–6804.
25 R. Tenne, L. Margulis, M. Genut and G. Hodes, *Nature*, 1992, **360**, 444–446.
26 M. Hershfinkel, L. Gheber, V. Volterra, J. Hutchison, L. Margulis and R. Tenne, *J. Am. Chem. Soc.*, 1994, **116**, 1914–1917.
27 Y. Feldman, E. Wasserman, D. Srolovitz and R. Tenne, *Science*, 1995, **267**, 222.
28 Y. Golan, C. Drummond, M. Homyonfer, Y. Feldman, R. Tenne and J. Israelachvili, *Adv. Mater.*, 1999, **11**, 934–937.
29 L. Rapoport, V. Leshchinsky, I. Lapsker, Y. Volovik, O. Nepomnyashchy, M. Lvovsky, R. Popovitz-Biro, Y. Feldman and R. Tenne, *Wear*, 2003, **255**, 785–793.
30 R. Rosentsveig, A. Gorodnev, N. Feuerstein, H. Friedman, A. Zak, N. Fleischer, J. Tannous, F. Dassenoy and R. Tenne, *Tribol. Lett.*, 2009, **36**, 175–182.
31 R. Rosentsveig, A. Margolin, A. Gorodnev, R. Popovitz-Biro, Y. Feldman, L. Rapoport, Y. Novema, G. Naveh and R. Tenne, *J. Mater. Chem.*, 2009, **19**, 4368–4374.
32 J. Tannous, F. Dassenoy, I. Lahouij, T. Le Mogne, B. Vacher, A. Bruhács and W. Tremel, *Tribol. Lett.*, 2011, **41**, 55–64.
33 L. Yadgarov, V. Petrone, R. Rosentsveig, Y. Feldman, R. Tenne and A. Senatore, *Wear*, 2013, **297**, 1103–1110.
34 C. Ballif, M. Regula, P. Schmid, M. Remškar, R. Sanjines and F. Levy, *Appl. Phys. A: Mater. Sci. Process.*, 1996, **62**, 543–546.
35 L. Yadgarov, R. Rosentsveig, G. Leitus, A. Albu-Yaron, A. Moshkovich, V. Perfilyev, R. Vasic, A. I. Frenkel, A. N. Enyashin and G. Seifert, *Angew. Chem., Int. Ed.*, 2012, **51**, 1148–1151.
36 A. Zak, L. Sallacan-Ecker, A. Margolin, M. Genut and R. Tenne, *Nano: Brief Rep. Rev.*, 2009, **4**, 91–98.
37 R. Levi, O. Bitton, G. Leitus, R. Tenne and E. Joselevich, *Nano Lett.*, 2013, **13**, 3736–3741.
38 R. Levi, J. Garel, D. Teich, G. Seifert, R. Tenne and E. Joselevich, *ACS Nano*, 2015, **9**, 12224–12232.
39 Y. Divon, R. Levi, J. Garel, D. Golberg, R. Tenne, A. Ya'akobovitz and E. Joselevich, *Nano Lett.*, 2016, **17**, 28–35.
40 F. Qin, W. Shi, T. Ideue, M. Yoshida, A. Zak, R. Tenne, T. Kikitsu, D. Inoue, D. Hashizume and Y. Iwasa, *Nat. Commun.*, 2017, **8**, 14465.
41 B. Visic, L. S. Panchakarla and R. Tenne, *J. Am. Chem. Soc.*, 2017, **139**, 12865–12878.
42 J. Wilson and A. Yoffe, *Adv. Phys.*, 1969, **18**, 193–335.
43 Footnote: the WS_2 nanotubes were acquired from ''Nano-Materials Ltd''.
44 L. Scheffer, R. Rosentzveig, A. Margolin, R. Popovitz-Biro, G. Seifert, S. Cohen and R. Tenne, *Phys. Chem. Chem. Phys.*, 2002, **4**, 2095–2098.
45 G. L. Frey, R. Tenne, M. J. Matthews, M. S. Dresselhaus and G. Dresselhaus, *J. Mater. Res.*, 1998, **13**, 2412–2417.
46 C. Ballif, M. Regula and F. Levy, *Sol. Energy Mater. Sol. Cells*, 1999, **57**, 189–207.
47 Footnote: From this point forward, the notation NW refers to cylindrical nanostructure with no empty core. Contrary, the notation NT refers to the cylindrical nanostructure with empty core.
48 Y. Li, A. Chernikov, X. Zhang, A. Rigosi, H. M. Hill, A. M. van der Zande, D. A. Chenet, E.-M. Shih, J. Hone and T. F. Heinz, *Phys. Rev. B: Condens. Matter Mater. Phys.*, 2014, **90**, 205422.
49 Footnote: The concept of ''Transparency dips'' refer to the splitting of the cavity resonances which appear near the wavelength associated with the A and B excitons.
50 X. Wu, S. K. Gray and M. Pelton, *Opt. Express*, 2010, **18**, 23633–23645.
51 G. Khitrova, H. Gibbs, M. Kira, S. Koch and A. Scherer, *Nat. Phys.*, 2006, **2**, 81–90.
52 A. Chernikov, T. C. Berkelbach, H. M. Hill, A. Rigosi, Y. Li, O. B. Aslan, D. R. Reichman, M. S. Hybertsen and T. F. Heinz, *Phys. Rev. Lett.*, 2014, **113**, 076802.

53 G. L. Frey, S. Elani, M. Homyonfer, Y. Feldman and R. Tenne, *Phys. Rev. B: Condens. Matter Mater. Phys.*, 1998, **57**, 6666–6671.
54 Footnote: The angle between the incident light and the normal of the film.
55 T. Tiedje, E. Yablonovitch, G. D. Cody and B. G. Brooks, *IEEE Trans. Electron Devices*, 1984, **31**, 711–716.
56 P. Sheng, *IEEE Trans. Electron Devices*, 1984, **31**, 634–636.
57 S. Itzhakov, H. Shen, S. Buhbut, H. Lin and D. Oron, *J. Phys. Chem. C*, 2013, **117**, 22203–22210.
58 K. Suzuki, *Nat. Photonics*, 2011, **5**, 247.
59 W. Liang, *Phys. Lett. A*, 1967, **24**, 573–574.

